ChemComm

COMMUNICATION

View Article Online
View Journal | View Issue

Cite this: *Chem. Commun.*, 2026, **62**, 5462

Received 12th January 2026,
Accepted 18th February 2026

DOI: 10.1039/d6cc00226a

rsc.li/chemcomm

Atomically dispersed Ru–Co pairs on hollow carbon as robust catalysts for the acidic oxygen evolution reaction

Fengqin Zhang,[a] Qingmei Wang, *[a] Zhijie Chen *[b] and Shun Lu *[c]

Developing durable, high-activity acidic oxygen evolution catalysts remains difficult. Here, we present atomically dispersed, spatially neighboring Ru–Co pairs anchored on hollow S,N-doped carbon *via* robust coordination. RuCo/SNC achieves a superior overpotential of 230 mV at 10 mA cm^{-2} and remarkable stability compared to RuO_2. *Operando* spectroscopy detects concurrent *OOH and *O–O intermediates, revealing a mechanism where adsorbate evolution coexists with moderated lattice oxygen participation. This cooperative pathway significantly suppresses metal leaching. Consequently, engineering anchored, electronically coupled Ru–Co pairs provides an effective strategy to regulate reaction pathways and overcome activity–stability trade-off in acidic oxygen evolution.

Electrocatalytic water splitting *via* proton-exchange membrane electrolyzers is pivotal for sustainable hydrogen production, yet it is hindered by the sluggish kinetics and instability of the oxygen evolution reaction (OER) in acidic media.[1–6] While RuO_2 and IrO_2 serve as benchmarks, they suffer from high costs and severe degradation due to metal dissolution and lattice oxygen loss.[7,8] Enhancing intrinsic activity often involves triggering the lattice oxygen oxidation mechanism (LOM), which bypasses the scaling limitations of the conventional adsorbate evolution mechanism (AEM). However, LOM participation typically accelerates lattice collapse, establishing a persistent trade-off between activity and stability.[9–17]

Atomically dispersed metal catalysts, particularly those featuring neighboring metal pairs, offer a precise platform to modulate electronic structures and break scaling relations.[18–21] Despite their potential, engineering such pairs to cooperatively moderate lattice oxygen activity, enhancing kinetics without inducing catastrophic structural failure, remains a major challenge.[22,23]

Herein, we address this by designing atomically dispersed Ru–Co pairs anchored on hollow S,N-doped carbon (RuCo/SNC). The hollow architecture facilitates mass transport, while robust M–N/M–S coordination stabilizes the metal sites. Using aberration-corrected microscopy and synchrotron spectroscopy, we confirm the formation of neighboring, electronically coupled Ru–Co centers. Operando spectroscopy and electrochemical studies reveal that this unique configuration promotes a balanced mechanism where AEM steps coexist with moderated LOM participation. This synergy yields superior acidic OER activity and significantly suppresses metal leaching, providing a robust strategy for designing durable catalysts.

In Fig. 1a, hollow SNC spheres hosting atomically dispersed Ru and Co species were constructed *via* a hard-templating strategy. Monodisperse SiO_2 cores were coated with S-doped polydopamine (SiO_2@SPDA), followed by metal precursor adsorption. Pyrolysis at 800 °C under N_2 converted SPDA into SNC, simultaneously immobilizing Ru and Co centers *via* robust M–N/M–S coordination. Subsequent HF etching removed the silica core, yielding hollow mesoporous spheres with abundant intra-shell nanopores. Notably, carbon is not electrochemically inert under acidic OER conditions; if local potential and defect density are not well controlled, carbon corrosion can compete with OER. Here, a hollow carbon framework is used to mitigate this, enabling the hollow S,N-doped carbon support to remain chemically stable above 1.5 V *vs.* reversible hydrogen electrode (RHE). This architecture, combined with polar S/N functionalities, enhances wettability and electrolyte accessibility. These structural features facilitate interfacial charge transport, and the hollow carbon framework further provides system-level benefits, including improved mass transport, regulated current distribution, facilitated bubble release, and mitigation of local current hotspots that could otherwise accelerate degradation.

[a] *Guizhou University Key Laboratory of Green Chemical and Clean Energy Technology, Guizhou University Engineering Research Center of Efficient Utilization for Industrial Waste, School of Chemistry and Chemical Engineering, Guizhou University, Institute of Dual-carbon and New Energy Technology Innovation and Development of Guizhou Province, Guiyang, Guizhou, 550025, China. E-mail: qmwang3@gzu.edu.cn*

[b] *Water Research Centre, School of Civil and Environmental Engineering, The University of New South Wales, Sydney, NSW 2052, Australia. E-mail: zhijie.chen1@unsw.edu.au*

[c] *Chongqing Institute of Green and Intelligent Technology, Chinese Academy of Sciences, Chongqing 400714, China. E-mail: lushun@cigit.ac.cn*

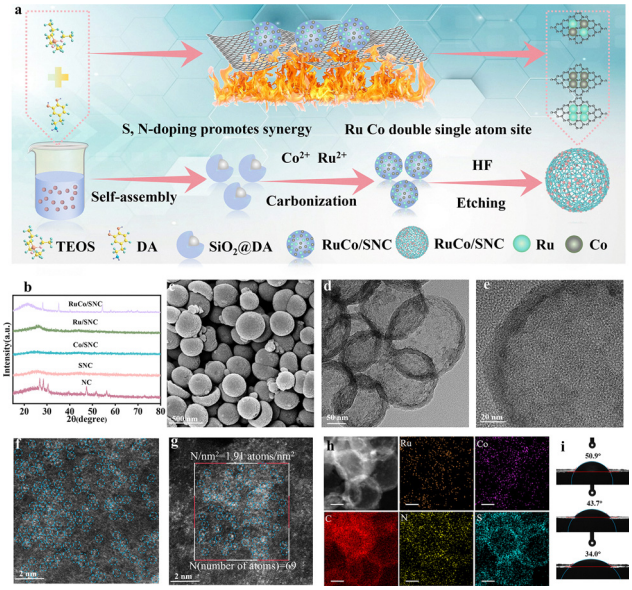

Fig. 1 (a) Synthetic scheme of Ru/SNC, Co/SNC and RuCo/SNC. (b) XRD patterns, (c) SEM image, (d) and (e) TEM images, (f) AC-HAADF-STEM images, (g) atomic density plot, (h) EDS elemental mapping, scale bar: 50 nm. (i) Contact angles, of Co/SNC, Ru/SNC, and RuCo/SNC (from top to down).

X-ray diffraction (XRD) patterns of RuCo/SNC (Fig. 1b) exhibit only broad diffraction features at ~25° indexed to graphitic carbon (002), with no reflections for crystalline metal phases, indicating the absence of long-range ordered metal species and high dispersion.[24] Scanning and transmission electron microscopy images (SEM/TEM, Fig. 1c–e) reveal hollow carbon nanospheres (average diameter ~102.7 nm; shell thickness ~15 nm). This thin and porous shell architecture provides internal void space and short diffusion pathways. Additionally, Barrett–Joyner–Halenda analysis shows a mesopore-centered pore size distribution (Fig. S1a). The N_2 adsorption–desorption isotherm displays a type-IV profile with an H3 hysteresis loop, confirming a hierarchical porous structure with a BET surface area of 179 m^2 g^{-1} (Fig. S1b).[25,26] Notably, this surface area is a deliberately designed, sufficiently high yet moderate choice that avoids exacerbating carbon corrosion and capacitive interference during OER while balancing practicality and long-term stability.

Aberration-corrected high-angle annular dark-field scanning transmission electron microscopy (AC-HAADF-STEM) images (Fig. 1f) reveal numerous isolated atom-like bright features uniformly distributed across the carbon framework, confirming atomic-level dispersion. Statistical analysis (Fig. 1g) indicates a high surface density of metal sites (1.91 atoms nm^{-2}), suggesting a high probability of short inter-site distances. Although Z-contrast alone does not distinguish Ru from Co, the observed atomic proximity, together with the equimolar Ru/Co ratio and subsequent XAS analysis, strongly supports the formation of neighboring Ru–Co configurations rather than isolated single-metal sites.[27,28] Automated spot recognition (Fig. S2) confirms that these features are well-isolated without lattice periodicity, ruling out nanocrystalline particles. Nearest-neighbor distance statistics (Fig. S3) exhibit a narrow distribution centered at 0.236 ± 0.008 nm. This distance is significantly shorter than expected for randomly distributed isolated atoms but lacks the ordering of metallic clusters, consistent with atomically dispersed neighboring pairs. Elemental mapping by energy-dispersive X-ray spectroscopy (STEM-EDS, Fig. 1h and Fig. S4) confirms the homogeneous distribution of Ru, Co, C, N, S, and O throughout the hollow shells. The corresponding spectrum (Fig. S5) validates the coexistence of these elements without detectable metallic impurities, and semi-quantitative analysis reveals comparable Ru and Co intensities consistent with the precursor stoichiometry. Finally, contact-angle measurements (Fig. 1i) show that RuCo/SNC exhibits a more hydrophilic surface (34.0°) than Ru/SNC (43.7°) and Co/SNC (50.9°), indicating enhanced wettability favorable for electrolyte contact.[29]

The electronic structure and local coordination environment of the RuCo/SNC catalyst were comprehensively analyzed using XPS and XAS. The XPS survey spectrum (Fig. S6) and quantitative analysis (Table S1) confirm the presence of Ru, Co, S, N, C, and O, with a surface Ru/Co atomic ratio (1.33 : 1.20) closely matching the precursor stoichiometry. High-resolution spectra reveal significant electronic interactions between the metal centers and the support. In the C 1s/Ru 3d region (Fig. 2a), the Ru 3d binding energy exhibits a negative shift relative to Ru/SNC, indicative of an electron-enriched Ru state. This electron enrichment, arising from synergistic coupling with neighboring Co atoms and the N/S-doped carbon matrix, is critical for

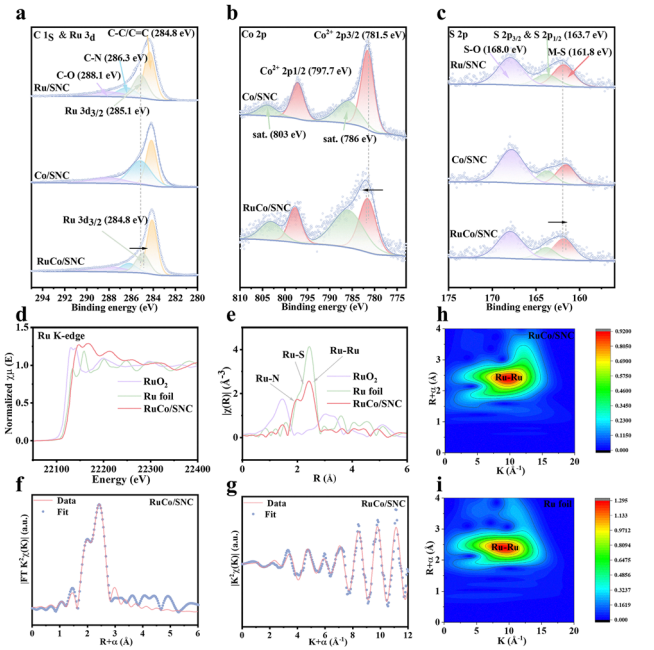

Fig. 2 High-resolution XPS spectra of (a) C 1s and Ru 3d, (b) Co 2p; (c) S 2p. (d) Normalized Ru K-edge XANES spectra of RuCo/SNC, Ru foil, and RuO_2, (e) comparison of Ru K-edge FT-EXAFS spectra (k^3-weighted) for RuCo/SNC, Ru foil, and RuO_2, (f) R-space fitting results of Ru K-edge EXAFS for RuCo/SNC, (g) k-space fitting results of Ru K-edge EXAFS for RuCo/SNC, (h) comparison of Ru K-edge WT-EXAFS contour plots for RuCo/SNC and (i) Ru foil.

acidic OER; it downshifts the Ru d-band center, optimizing the binding strength of oxygenated intermediates and mitigating the risk of over-oxidation and lattice oxygen loss.[30–32] Conversely, the Co 2p spectrum (Fig. 2b) shows a positive shift and weakened satellite features, suggesting electron donation and strong covalency in Co–N/S bonds. This electronic asymmetry confirms the formation of electronically coupled Ru–Co pairs.[33]

The coordination environment is further elucidated by the S 2p (Fig. 2c) and N 1s (Fig. S7a) spectra, which display dominant metal–S and metal–N contributions, respectively. Notably, the N dopants serve as acid-tolerant anchoring sites by forming M–N bonds, and these strong interaction sites anchor the metal species, preventing atomic migration and aggregation under acidic OER conditions. Meanwhile, S dopants provide a softer, more covalent coordination that reduces the ionic character of Ru–O bonding and mitigates oxidative bond cleavage, which is expected to primarily contribute to durability. Additionally, O 1s spectra (Fig. S7b) reveals lattice M–O and surface M–OH species contributing to hydrophilicity, with long-term durability mainly arising from the comparatively stable M–N/M–S coordination rather than labile oxygenated groups. Raman spectroscopy (Fig. S8) indicates a high defect density (I_D/I_G = 1.23) in the carbon framework, providing rich sites for metal anchoring.

Synchrotron-based Ru K-edge XAS provided element-specific structural insights. The XANES spectra (Fig. 2d) show that the absorption edge of RuCo/SNC aligns closer to RuO_2 than Ru foil, confirming Ru exists in a partially oxidized state. The white-line intensity reflects the depletion of Ru 4d electrons due to coordination with electronegative heteroatoms (N/S).[34] In the Fourier-transformed EXAFS (FT-EXAFS) spectra (Fig. 2e), RuCo/SNC lacks the prominent Ru–Ru peak at 2.65 Å observed in Ru foil, indicating the absence of extended metallic domains. Instead, the profile is dominated by light-element scattering in the first shell. Notably, an individual Ru–Co scattering contribution cannot be unambiguously resolved from the Ru K-edge FT-EXAFS under our experimental conditions due to the low coordination number and limited *R*-space resolution. Quantitative fitting (Fig. 2f, g and Table S2) identifies the primary coordination sphere as Ru–N ($R \approx 1.92$ Å) and Ru–S ($R \approx 2.30$ Å). For completeness, a weak Ru–Ru path was included in the fitting model. However, given its subtle contribution and the lack of an apparent Ru–Ru feature in the FT-EXAFS, this should not be taken as direct evidence of metallic Ru clustering, but rather as possible short-range correlations among sparsely distributed metal centers. A minor Ru–Ru scattering path is also resolved; however, given the absence of metallic diffraction peaks and the attenuated FT intensity, this is attributed to short-range correlations between neighboring single atoms rather than metallic clustering. Reference fits for Ru foil and RuO_2 are provided in Fig. S9, supporting the fitting strategy. This interpretation is corroborated by Wavelet Transform EXAFS (WT-EXAFS) (Fig. 2h), which shows intensity maxima at low *k*-values characteristic of light-element backscattering, distinct from the high-*k* metallic Ru–Ru features (Fig. 2i), while RuO_2 (Fig. S10) provides a reference for Ru–O-dominated scattering features. Collectively, these spectroscopic data confirm atomically dispersed Ru stabilized by heteroatom coordination within an electronically coupled Ru–Co configuration.

The OER activity of RuCo/SNC was evaluated in 0.5 M H_2SO_4 against commercial RuO_2 and control samples. RuCo/SNC delivers superior activity, requiring an overpotential of 230 mV to reach 10 mA cm^{-2} (η_{10} = 230 mV; Fig. 3a), significantly outperforming RuO_2 (260 mV) and single-metal counterparts. The enhanced activity is observed across a broad current density range (Fig. 3b) and is further improved by HF etching, which removes surface residues to expose active sites and facilitate mass transport (Fig. S11–S13). The reaction kinetics are favorable, evidenced by a low Tafel slope of 76.6 mV dec^{-1} (Fig. 3c) and a charge-transfer resistance of 42.1 Ω, the lowest among tested catalysts (Fig. 3d). Furthermore, RuCo/SNC exhibits a high double-layer capacitance (C_{dl}) of 33.4 mF cm^{-2} (Fig. 3e and Fig. S14), indicating a larger electrochemically accessible surface area. In Fig. 3f, RuCo/SNC exhibits a higher performance than other acidic OER catalysts. In terms of stability, the catalyst sustains stable operation for 40 hours (Fig. S15), demonstrating durability superior to commercial RuO_2 under acidic conditions. Post-OER characterizations further confirm that hollow carbon framework and atomically dispersed Ru species are well preserved after the durability test (Fig. S16). RuCo/SNC also shows exceptional HER activity, with η_{10} = 37.4 mV and a Tafel slope of 39.1 mV dec^{-1} (Fig. 3g and h), comparable to Pt/C. Long-term measurement confirms its robustness, with negligible degradation over 108 hours (Fig. 3i). These results highlight RuCo/SNC as a highly efficient and durable bifunctional catalyst for acidic water splitting.

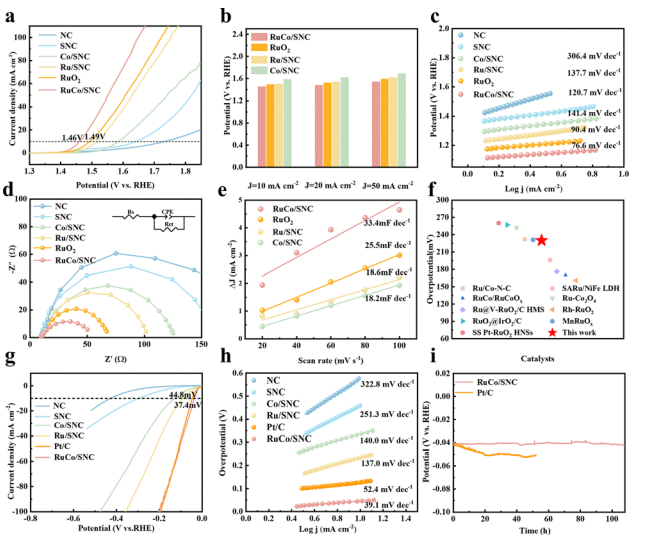

Fig. 3 OER analysis: (a) LSV curves, (b) potentials at given current densities, (c) Tafel plots, (d) Nyquist plots (data were fitted using the equivalent circuit shown in the inset. *iR* correction was applied using partial compensation, with the solution resistance (R_s) determined from the high-frequency intercept), (e) double-layer capacitance from non-faradaic CV curves. (f) Comparison of OER activity of RuCo/SNC with other reported catalysts. (literature values are for contextual reference only and should be considered semi-quantitative). HER analysis: (g) LSV curves, (h) Tafel plots, (i) Stability test on carbon cloth at 50 mA cm^{-2}.

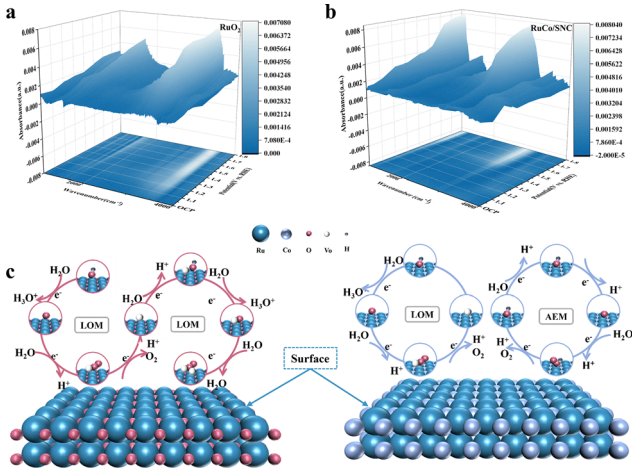

Fig. 4 3D ATR-FTIR surface plot at different potentials with the corresponding 2D projection of (a) RuO_2, and (b) RuCo/SNC. (c) Schematic illustration of possible OER pathways.

To reveal OER reaction pathway, *operando* ATR-SEIRAS (Attenuated total reflectance surface-enhanced infrared absorption spectroscopy) was performed on RuCo/SNC and commercial RuO_2 from OCP to 1.8 V *vs.* RHE. The spectra for RuO_2 (Fig. 4a, b and Fig. S17a) are dominated by broad –OH/H_2O features without discernible *O–O bands, consistent with the severe lattice instability often observed in benchmark oxides. In contrast, RuCo/SNC exhibits distinct vibrational bands emerging at ~1146 cm^{-1} and ~1192 cm^{-1} as the anodic potential increases (Fig. S17b). Following widely adopted operando ATR-SEIRAS results for acidic Ru-based OER catalysts, and noting that exact band positions may vary with the local adsorption environment, these features are assigned to *OOH and *O–O intermediates, respectively.[35,36] The simultaneous persistence of *OOH and *O–O signals over a broad potential window suggests a hybrid reaction scenario: conventional proton-coupled electron transfer steps (AEM) coexist with partial lattice oxygen participation (LOM), rather than a single dominant pathway (Fig. 4c). This hybrid reaction behavior originates from Ru centers within neighboring Ru–Co motifs that support AEM, together with adjacent Co and N/S coordination environment that weakens and optimizes Ru–O bonding by regulating local electronic structures, thereby enabling limited lattice-oxygen participation associated with LOM.[37–40]

To verify if this lattice involvement compromises stability, metal dissolution was quantified after 40 h of operation (Table S3). Remarkably, RuCo/SNC exhibits substantially lower Ru leaching compared to commercial RuO_2, despite the spectroscopic signature of lattice oxygen species. While RuO_2 suffers from severe dissolution typically driven by excessive lattice oxidation and Ru–O bond cleavage, the suppressed metal release in RuCo/SNC indicates that lattice participation is effectively moderated. This implies that the robust heteroatom anchoring and electronic coupling within the Ru–Co pairs induce local electron redistribution, modulate Ru–O bonding, and help suppress over-oxidation and dissolution, thereby mitigating the catastrophic structural degradation often associated with LOM and stabilizing the catalyst under acidic conditions.

In summary, we developed a RuCo/SNC catalyst for acidic OER by anchoring electronically coupled Ru–Co atom pairs on hollow S,N-doped carbon. The hollow architecture enhances mass transport, while heteroatom coordination stabilizes metal centers and induces local electron redistribution that modulates Ru–O bonding, suppresses metallic aggregation, and mitigates over-oxidation and dissolution. RuCo/SNC achieves high activity (η_{10} = 230 mV) and markedly improved durability over RuO_2. *Operando* ATR-SEIRAS reveals concurrent *OOH and *O–O intermediates formation, indicating a cooperative regime that couples adsorbate-mediated steps with moderated lattice oxygen participation, thereby alleviating the activity–stability trade-off and suppressing Ru dissolution. Therefore, engineering local coordination environments in neighboring single-atom pairs is a viable strategy for designing high-performance Ru-based catalysts for acidic water oxidation.

F. Zhang: investigation, data analysis and curation, writing – original draft. Q. Wang: project administration, funding acquisition, supervision. Z. Chen: investigation, writing – review and editing. S. Lu: funding acquisition, writing – review and editing.

Conflicts of interest

The authors declare no conflict of interest.

Data availability

The data supporting this article have been included as part of the supplementary information (SI). Supplementary information is available. See DOI: https://doi.org/10.1039/d6cc00226a.

Acknowledgements

This research work was financially supported by Nature Science Foundation of China (No. 52200076, 22169005 and 22408067), Key Project of Guizhou Province Basic Research Program (ZD-[2025]-077), Guizhou Science and Technology Platform foundation (No. ZSYS 412 [2025]-033),and the Special Research Fellowship of the Chinese Academy of Science (No. E3296201).

References

1 Y. Gao, C. Yang, X. Zheng, Z. Zhuang, J. Yang, Y. Dou, J. Zhang and D. Wang, *J. Am. Chem. Soc.*, 2025, **147**, 18760–18769.
2 X. Liu, W. Zhang, X. Wu and Y.-R. Cho, *Energy Mater. Adv.*, 2025, **6**, 0160.
3 C. Yang, Q. Wang, Y. Xiong, T. Zhang, Z. Zhu, Y. Zeng and S. Lu, *Langmuir*, 2025, **41**, 33525–33531.
4 K. N. Nguyen, T. N. N. Tran, K. T. T. Tran, M. V. Tran, N. H. Vu, T.-T. Nguyen, Y. Kawazoe and V. V. Pham, *Energy Mater. Adv.*, 2025, **6**, 0162.
5 Y. Han, Q. Wang, F. Zhang, Q. Hua and S. Lu, *Chem. Commun.*, 2026, **62**, 620–624.
6 Y. Mu, X. Pei, Y. Zhao, X. Dong, Z. Kou, M. Cui, C. Meng and Y. Zhang, *Nano Mater. Sci.*, 2023, **5**, 351–360.
7 S. Kuang, X. Lu, J. Wang, H. Lin and Q. Li, *Prog. Chem.*, 2025, **37**, 1581–1603.
8 J. Liu, J. Yang, Y. Dou, X. Liu, S. Chen and D. Wang, *Adv. Mater.*, 2025, **37**, 2420383.

9 W. Li, D. Chen, Z. Lou, H. Yuan, X. Fu, H. Y. Lin, M. Lin, Y. Hou, H. Qi, P. F. Liu, H. G. Yang and H. Wang, *J. Am. Chem. Soc.*, 2025, **147**, 10446–10458.
10 L. Wang, S. F. Hung, S. Zhao, Y. Wang, S. Bi, S. Li, J. J. Ma, C. Zhang, Y. Zhang, L. Li, T. Y. Chen, H. Y. Chen, F. Hu, Y. Wu and S. Peng, *Nat. Commun.*, 2025, **16**, 3502.
11 W. Zheng, X. Cheng, P. Chen, L. Wang, Y. Duan, G. Feng, X. Wang, J. Li, C. Zhang, Z. Yu and T. Lu, *Nat. Commun.*, 2025, **16**, 337.
12 S. Lu, X. Zheng, K. Jiang, Q. Wang, X. Wang, M. Shahzad, F. Yin, B. Xu, Q. Hua and H. Liu, *Adv. Compos. Hybrid Mater.*, 2025, **8**(2), 182.
13 B. Yuan, Q. Dang, H. Liu, M. G. Sendeku, J. Peng, Y. Fan, L. Cai, A. Cao, S. Chen, H. Li, Y. Kuang, F. Wang and X. Sun, *Nat. Commun.*, 2025, **16**, 4583.
14 K. Ji, S. Wang, S. Yao, Y. Ji, J. Li, X. Wang, L. Shi, G. Wang, W. Ren, J. Wang, F. Zhang, J. Xie, Z. Yang and Y. Yan, *Adv. Mater.*, 2025, **37**, e2503182.
15 H. Wang, C. Lin, L. Tan, J. Shen, X. Wu, X. Pan, Y. Zhao, H. Zhang, Y. Sun, B. Mei, H. D. Um, Q. Xiao, W. Jiang, X. Li and W. Luo, *Nat. Commun.*, 2025, **16**, 3976.
16 C. Yang, Y. Zhu, F. Zhang, Y. Yao, Y. Chen, T. Lu, Q. Li, J. Li, G. Wang, Q. Cheng and H. Yang, *Adv. Mater.*, 2025, **37**, e2507560.
17 Y. Zhu, F. Wu, X. Zhang, Y. Lin, L. Zhang, T. S. Chan, Q. Zhang and L. Chen, *Adv. Mater.*, 2025, **37**, e2500449.
18 X. Zheng, Z. Wang, Q. Zhou, Q. Wang, W. He and S. Lu, *J. Energy Chem.*, 2024, **88**, 242–251.
19 Y. Cong, L. Chen, Z. Dai, M. Liu, H. Wang, X. Zhou, Q. Zhao and C. Li, *Adv. Funct. Mater.*, 2025, **35**, e12538.
20 Z. Jiang, L. Shao, Y. Sun, Y. Dong, X. Zheng, T. Wang, J. Li, H. Shao, L. Jiao and Y. Deng, *Adv. Funct. Mater.*, 2025, **35**, e09656.
21 Y. Liu, Y. Wang, H. Li, M. G. Kim, Z. Duan, K. Talat, J. Y. Lee, M. Wu and H. Lee, *Nat. Commun.*, 2025, **16**, 1717.
22 X. He, M. Liu, F. Liu, X. Liu, H. Liao, P. Tan and J. Pan, *Adv. Funct. Mater.*, 2025, **35**, e05936.
23 Y. Mu, D. Zhang, T. Gao, L. Wang, L. Zhang, X. Zou, W. Zheng, J. Fan and X. Cui, *Angew. Chem., Int. Ed.*, 2025, **64**, e202505908.
24 R. Wu, J. Zuo, C. Fu, Z. Zhu, L. Zhao, J. Wang, Q. Li, Q. Xue, Z. Li, X. Niu, X. Qi, N. Yang and J. S. Chen, *ACS Nano*, 2025, **19**, 20215–20224.
25 X. Tian, R. Liu, W. Wang, Q. Yang, Z. Huang, Y. Yang, J. Han, T. Dong, Y. Du, J. Lai, H. Li and L. Wang, *Adv. Mater.*, 2025, **37**, e06068.
26 Y. Xu, W. Zhao, R. Chen, H. Li, X. Liu, P. Wu, H. Yu, J. Wang, L. L. Shen, G. R. Zhang and D. Mei, *Adv. Funct. Mater.*, 2026, **36**, e12498.
27 F. Jiang, Y. Li and Y. Pan, *Adv. Mater.*, 2024, **36**, e2306309.
28 Y. Chen, H. Bai, J. Lan, C. W. Kao, F. Xie, L. Meng, J. Li, Y. R. Lu, M. Peng, H. Pan and Y. Tan, *Angew. Chem., Int. Ed.*, 2025, **64**, e202504568.
29 P. Yu, L. Wang, F. Sun, Y. Xie, X. Liu, J. Ma, X. Wang, C. Tian, J. Li and H. Fu, *Adv. Mater.*, 2019, **31**, 1901666.
30 M. You, X. Du, X. Hou, Z. Wang, Y. Zhou, H. Ji, L. Zhang, Z. Zhang, Y. Yi and D. Chen, *Appl. Catal., B*, 2022, **317**, 121729.
31 Z. Li, S. Ji, C. Wang, H. Liu, L. Leng, L. Du, J. Gao, M. Qiao, J. H. Horton and Y. Wang, *Adv. Mater.*, 2023, **35**, 2300905.
32 X. Zhao, G. Wu, X. Zheng, P. Jiang, J. D. Yi, H. Zhou, X. Gao, Z. Q. Yu and Y. Wu, *Angew. Chem., Int. Ed.*, 2023, **62**, e202300879.
33 K. Shah, R. Dai, M. Mateen, Z. Hassan, Z. Zhuang, C. Liu, M. Israr, W. C. Cheong, B. Hu, R. Tu, C. Zhang, X. Chen, Q. Peng, C. Chen and Y. Li, *Angew. Chem., Int. Ed.*, 2022, **61**, e202114951.
34 X. Cao, L. Miao, W. Jia, H. Qin, G. Lin, R. Ma, T. Jin and L. Jiao, *Nat. Commun.*, 2025, **16**, 6217.
35 W. Liao, F. Qing, Q. Liu, R. Wu, C. Zhou, L. Chen, Y. Chen and X. Li, *Nano Lett.*, 2025, **25**, 1575–1583.
36 L. Wang, S.-F. Hung, S. Zhao, Y. Wang, S. Bi, S. Li, J.-J. Ma, C. Zhang, Y. Zhang, L. Li, T.-Y. Chen, H.-Y. Chen, F. Hu, Y. Wu and S. Peng, *Nat. Commun.*, 2025, **16**, 3502.
37 L. Li, G. Zhang, C. Zhou, F. Lv, Y. Tan, Y. Han, H. Luo, D. Wang, Y. Liu, C. Shang, L. Zeng, Q. Huang, R. Zeng, N. Ye, M. Luo and S. Guo, *Nat. Commun.*, 2024, **15**, 4974.
38 H. Wu, J. Chang, J. Yu, S. Wang, Z. Hu, G. I. N. Waterhouse, X. Yong, Z. Tang, J. Chang and S. Lu, *Nat. Commun.*, 2024, **15**, 10315.
39 N. Yao, H. Jia, J. Zhu, Z. Shi, H. Cong, J. Ge and W. Luo, *Chem*, 2023, **9**, 1882–1896.
40 L. Li, G. Zhang, C. Zhou, F. Lv, Y. Tan, Y. Han, H. Luo, D. Wang, Y. Liu, C. Shang, L. Zeng, Q. Huang, R. Zeng, N. Ye, M. Luo and S. Guo, *Nat. Commun.*, 2024, **15**, 4974.

